Thickness-dependent anisotropic superconductivity and charge density wave in ZrTe₃ down to the two-dimensional limit

Xinyu Chen ◉,[1] Changsheng Zhu,[1] Bin Lei,[1] Weizhuang Zhuo,[1] Wenxiang Wang,[1] Jiaxiang Ma ◉,[1] Xigang Luo ◉,[1] Ziji Xiang,[1] and Xianhui Chen ◉[1,2,3,*]

[1]*Department of Physics, University of Science and Technology of China, and Key Laboratory of Strongly Coupled Quantum Matter Physics, Chinese Academy of Sciences, Hefei 230026, China*
[2]*CAS Center for Excellence in Superconducting Electronics (CENSE), Shanghai 200050, China*
[3]*CAS Center for Excellence in Quantum Information and Quantum Physics, Hefei, Anhui 230026, China*

Reduced thickness could have dramatic impact on the dynamic ordering kinetics and the electronic structures in two-dimensional materials. Here we focus on ZrTe₃, a quasi-one-dimensional charge-density-wave system that can transform into a mixed bulk-filament anisotropic superconducting state with the superconducting transition temperature (T_c^{zero}) of 1.6 K. We have successfully exfoliated ZrTe₃ crystal from bulk crystal to bilayer (2 nm) flake. By examining the anisotropic transport properties, we reveal a competitive relationship between superconductivity and charge density wave (CDW) in the thickness range down to 8 nm. With decreasing thickness, superconductivity is enhanced (yielding a maximum T_c^{zero} of about 5 K at 18 nm) while CDW is suppressed. Upon further decreasing thickness, an unexpected enhancement on CDW transition temperature was observed accompanied with the superconductivity rapidly suppressing and finally vanishing. Shifting of Fermi level upon thinning, anisotropic strain from the substrates, and the increase of disorder scattering as approaching the two-dimensional limit might be taken into account for understanding these behaviors. The nonmonotonic evolution with a reduction of thickness is rare and may indicate an intricate mechanism of CDW and SC in ZrTe₃.

I. INTRODUCTION

Until now, the competition and coexistence between charge density wave and superconductivity have been a focal point in the field of condensed matter physics [1,2]. In particular, layered van der Waals materials with a CDW transition have garnered significant attention due to their relatively easy exfoliation and more optional methods to modulate the electronic structure, yet many exotic physical properties and quantum states involved in CDW and SC have been investigated [3,4].

The transition metal trichalcogenides (TMTs) are a particular class of quasi-one-dimensional (Q1D) linear-chain compounds, which often show a CDW transition. Among them, ZrTe₃ stands out due to its novel structural and unusual physical properties [5–7]. It shows a charge density wave transition at 63 K with Peierls modulation $q \approx (\frac{1}{14}, 0, \frac{1}{3})$ and a highly anisotropic superconducting transition well below the CDW transition temperature [8]. The resistance along a axis starts to drop around 2.5 K, interpreted as a filamentary superconductivity induced by the local pairs [9], whereas the resistance along b axis decreases at a lower temperature. A mixed bulk-filament state was proposed to explain this anisotropy [10]. Band structure calculations and angle-resolved photoemission spectroscopy (ARPES) revealed a rounded three-dimensional Fermi surface (FS) sheet at the center of the Brillouin zone (BZ) and two flatter Q1D sheets parallel to the BZ boundary [11,12]. These 3D and Q1D FSs intersect and form a van Hove singularity (vHS). The Q1D FSs responsible for the CDW state and superconductivity are sensitive to the change in BZ size modulated by variation of the lattice constant [13]. Previous studies by adopting pressure, doping, and intercalation only focused on the competitive relation between CDW formation and superconductivity in the bulk crystals [14–17]. Given that the interlayer coupling strength is often varied when crystals are reduced to a few atomic layers, and the CDW formation and superconductivity can be drastically changed by varying electron-phonon coupling, it could be a unique perspective to explore layer-controlled transport properties in ZrTe₃ flakes down to the 2D limit.

In this work, we successfully exfoliate sizable ZrTe₃ nanoflakes with thickness ranging from a few hundred to two nanometers (bilayer) by using traditional mechanical and Al₂O₃-assisted exfoliation methods. The superconducting and CDW state can be consistently observed in samples with thicknesses above 8 nm, while those thinner than 8 nm show semiconducting behavior and no anomaly can be found even in the derivative dR/dT. As the thickness is reduced from bulk to 8 nm, T_c^{zero} first increases rapidly and slowly reaches its maximum at around 18 nm for both a and b directions, and then is suppressed rapidly. Further Hall measurements show that Hall resistivity (ρ_{xy}) is almost linearly dependent on magnetic field up to 9 T in the whole thickness range

*chenxh@ustc.edu.cn

and the evolution of carrier concentration inversely correlates with that of the CDW transition temperature. Shifting of Fermi level upon thinning, enhanced strains from substrate and disorder scattering as approaching the two-dimensional limit might be taken into account for these behaviors. We also took magnetoresistance measurements with magnetic field applied along the out-of-plane direction for $I \parallel a$ and $I \parallel b$, respectively. The upper critical fields (H_{c2}) can be modeled using the Ginzburg-Landau (GL) theory and we observed a similar temperature dependence of H_{c2} for current applied along a and b axes.

II. EXPERIMENTAL DETAILS

Single crystals of monoclinic ZrTe$_3$ were synthesized by an iodine vapor transport method [18]. Stoichiometric amounts of high purity Zr and Te powders were sealed with moderate iodine powder in a quartz tube under high vacuum. High-quality single crystals were found at the cold end of the tube after maintaining the quartz tube at a gradient temperature from 700 to 750 °C for 14 days. Sizable flakes thicker than 10 nanometers were obtained through exfoliating the bulk crystals mechanically and then transferred from the scotch tape onto the Si/SiO$_2$ substrate. An Al$_2$O$_3$-assisted exfoliation technique was used to get the thinner flakes [19]. First, the Al$_2$O$_3$ film was deposited onto a freshly cleaved surface of the bulk crystals by thermally evaporating and then a thermal-release tape was used to pick up Al$_2$O$_3$ film along with pieces of ZrTe$_3$ microcrystals separated from the bulk. The Al$_2$O$_3$/ZrTe$_3$ stack was subsequently released onto a piece of transparent polydimethylsiloxane (PDMS). Next, the PDMS/ZrTe$_3$/Al$_2$O$_3$ assembly was stamped onto a Si/SiO$_2$ substrate and then the PDMS was quickly peeled away, leaving the Al$_2$O$_3$ film covered with freshly cleaved ZrTe$_3$ flakes on the Si/SiO$_2$ substrate. Au (120 nm)/Cr (5 nm) electrodes were patterned onto the thin flakes for transport measurements. Due to the Q1D nature of ZrTe$_3$, the flakes exhibited a band-shaped appearance with sharp edges and the longer side of the flakes, as determined from optical images, aligned with the b axis. To prevent sample degradation, the flakes were encapsulated with hexagonal boron nitride thin flakes and the whole process above was done in an argon-filled glove box.

The thickness of the flakes was identified by an atomic force microscopy and the light contrast. Optical transmittance defined as $G^T_{sample}/G^T_{substrate}$ obeys the Beer-Lambert law, where G^T_{sample} and $G^T_{substrate}$ are the intensity of the transmission through the sample and substrate of the image captured with a CCD camera [20]. Electrical transport properties were measured in a commercial physical property measurement system (PPMS, by Quantum Design).

III. RESULTS AND DISCUSSION

The schematic crystal structure of ZrTe$_3$ is depicted in Fig. 1(a). It comprises infinite Q1D chains formed by ZrTe$_3$ trigonal prisms stacking along the b axis and the layers stack along the c axis by van der Waals forces [21], forming a monoclinic structure that allows exfoliation. Using mechanical and Al$_2$O$_3$-assisted exfoliation techniques, thin flakes of various thicknesses down to monolayer can be obtained, as illustrated
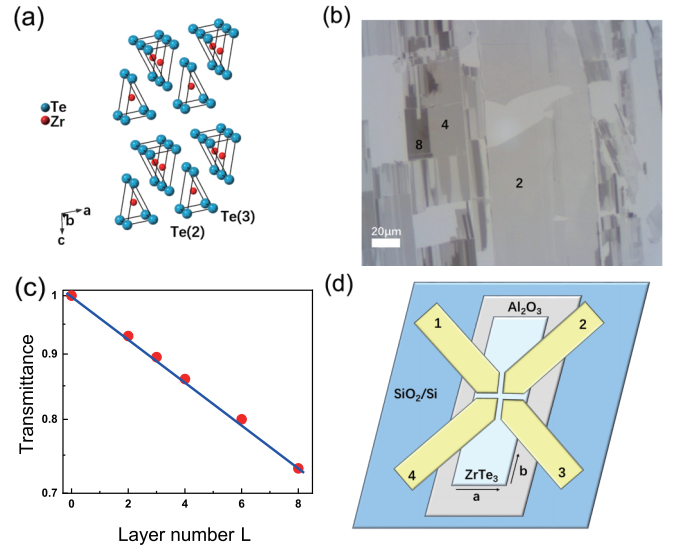
FIG. 1. (a) Schematic crystal structure of ZrTe$_3$. (b) Optical image of the exfoliated thin flakes of ZrTe$_3$ on the Al$_2$O$_3$ film (thickness 80 nm) attached to PDMS film. Image was taken in transmission mode. Number of layers is labeled on selected flakes. (c) Optical transmittance as a function of the number of layers. The transmittance follows the Beer-Lambert law. The transmittance is defined as $G^T_{sample}/G^T_{substrate}$, where G^T_{sample} and $G^T_{substrate}$ are the intensities of the transmission (T) through the sample and substrate of the image captured with a CCD camera. (d) A schematic illustration of the ZrTe$_3$ thin flake device. The electrodes are labeled by numbers. The current can flow along the a axis or b axis.

in Figs. 1(b) and 1(c). Figure 1(d) presents the schematic illustration of the ZrTe$_3$ thin flake device. In the resistivity measurements along the a axis (b axis), current was applied from electrode contact 1 to 2 (4), while voltage was measured by contact 4 (2) and 3. For Hall measurement, current was applied from electrode contact 1 to 3, while voltage was measured by contact 4 and 2. This approach enabled the collection of resistance data along two axes and the Hall signal from the same flake.

Figures 2(a) and 2(b) show the systematic thickness dependence of normalized resistance [$R(T)/R(200\ \mathrm{K})$] with current along the a and b axes, respectively. A clear resistance upturn corresponding to the CDW transition can be observed at 63 K in bulk crystal for $I \parallel a$ [9,18]. The CDW transition temperature (T_{CDW}) is then defined by the minimum point in the temperature-dependent differential resistance (dR/dT) as the current parallel to the a axis, as shown in Fig. 2(c). The superconducting transition emerges with zero resistance at $T_c^{zero} \approx 1.6$ K for a axis and 1.4 K for b axis. With decreasing thickness, the CDW transition can be observed in the resistance curve for the current along the a axis except the flakes thinner than 3 nm, as marked by the arrows in Fig. 2(a). The temperature derivative dR/dT [as shown in Fig. 2(c)] indicates that T_{CDW} decreases first and then increases with the reduction of thickness. For $I \parallel a$, while the thickness is reduced from bulk to 13 nm, T_c^{zero} initially increases significantly from 1.6 K to 5 K (at around 18 nm) and then decreases to 3.2 K, as shown in Fig. 3(a). For $I \parallel b$, the superconducting transition temperature exhibits a similar trend, with T_c^{zero}
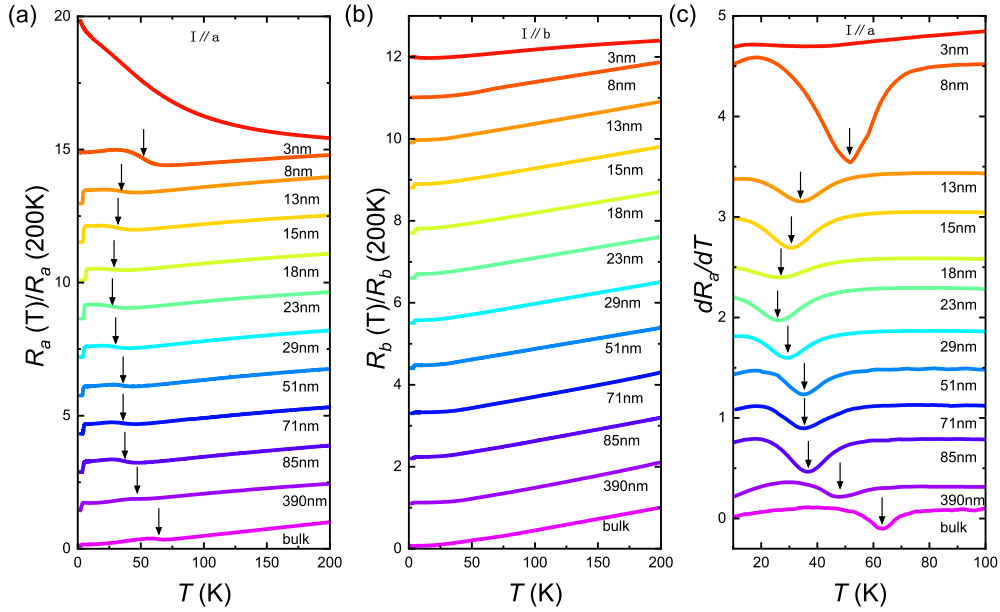
FIG. 2. (a), (b) Evolution of the temperature-dependent normalized resistance $R(\mathrm{T})/R(200\ \mathrm{K})$ for ZrTe$_3$ flakes from bulk to 3 nm ($3L$) with the current flow along the a axis (a) and the b axis (b). The arrows in (a) indicate the kink in the resistance curve, which corresponds to the CDW transition. (c) Temperature dependence of the normalized derivative of resistance $\mathrm{d}R/\mathrm{d}T$ in (a); the arrows indicate the position of the CDW transition, which is determined by the minimum point in the temperature dependent differential resistivity ($\mathrm{d}R/\mathrm{d}T$). The same color is used for the same thickness in (a), (b), and (c). All the curves were shifted vertically for clarity.

first increasing from 1.4 K to 4.2 K and then decreasing to 2.8 K, as shown in Fig. 3(b). Figures 3(c) and 3(d) show the temperature dependent resistance $R(T)/R(200\ \mathrm{K})$ of samples with different flake thickness of 2–8 nm. In the 8 nm thick flake, $R(T)$ shows a slight drop near 1.9 K for $I \parallel a$, which might be related to a superconducting transition, while resistance exhibits a metallic behavior throughout the temperature

range along the b axis. The $R(T)$ of thinner flakes shows a semiconducting behavior at low temperature.

In order to characterize the anisotropic superconductivity in ZrTe$_3$, magnetoresistance is measured with magnetic field applied along the c axis for both $I \parallel a$ and $I \parallel b$. Figures 4(a) and 4(b) show the temperature dependence of normalized resistance for $I \parallel a$ and $I \parallel b$ under different out-of-plane
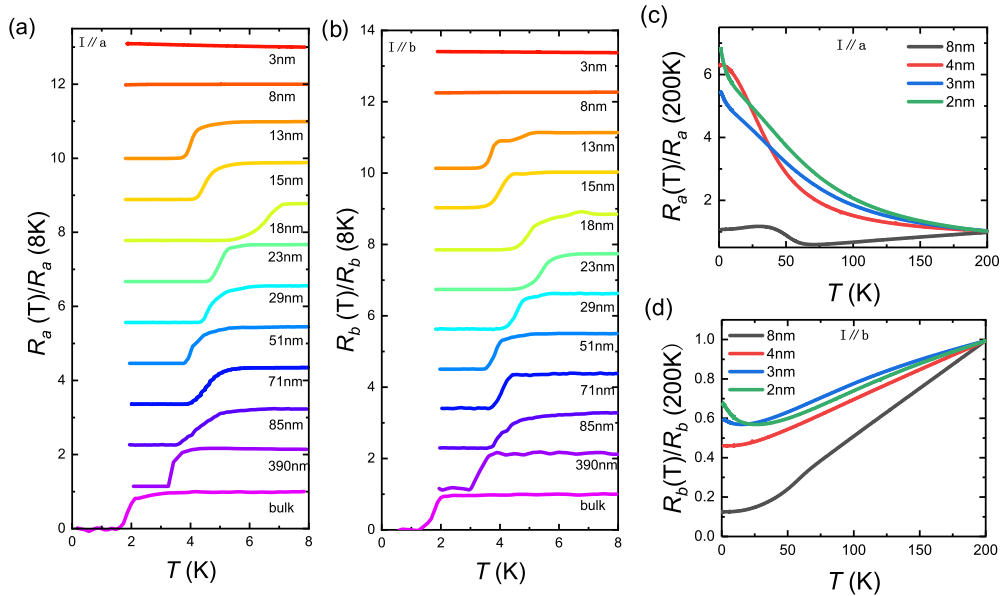
FIG. 3. (a), (b) Details of normalized resistance $R(\mathrm{T})/R(8\ \mathrm{K})$ with temperature range from 8 K to 1.8 K for watching the superconducting transition with the current flow along the a axis (a) and the b axis (b). All the curves in (a) and (b) were shifted vertically for clarity. T_c^{zero} is defined as the temperature at which resistance reaches zero. (c), (d) The details of normalized resistance $R(\mathrm{T})/R(200\ \mathrm{K})$ of ZrTe$_3$ flakes from 8–2 nm with the current flow along the a axis (c) and the b axis (d). Monolayer ZrTe$_3$ turns out to be an insulator and its resistance cannot be measured.
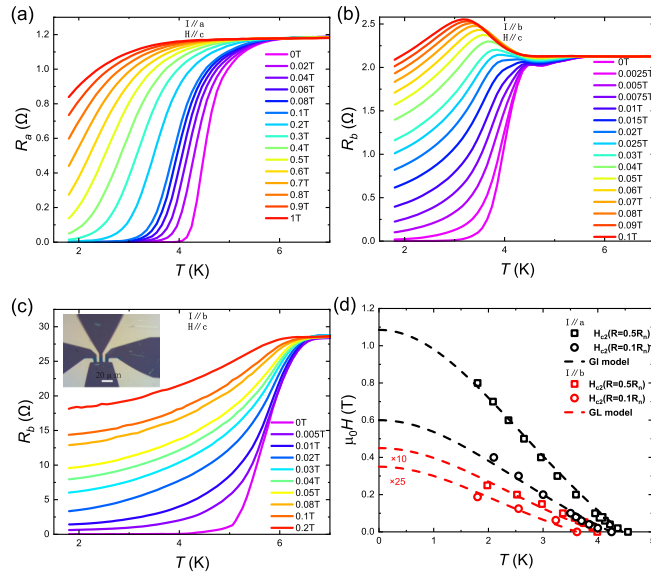
FIG. 4. (a), (b) Temperature-dependent resistance of the flake with thickness of 15 nm under different out-of-plane magnetic fields with the current flow along the a axis (a) and the b axis (b). (c) Temperature-dependent resistance under various out-of-plane magnetic fields with the current flow along the b axis, measured by the standard four-probe method for comparison. Inset is the schematic illustration of the ZrTe$_3$ thin flake device. (d) Temperature-dependent $H_{c2}(R = 0.5R_n)$ (square) and $H_{c2}(R = 0.1R_n)$ (circle) with magnetic field applied along out-of-plane directions. Dashed curves are theoretical curves obtained from the 2D Ginzburg-Landau equations.

magnetic fields in a flake with thickness of 15 nm. When the magnetic field increases, T_c^{zero} is shifted to the low temperature side and the transition width becomes broader [10]. Superconductivity along the b axis is much more sensitive than that along the a axis. For $I \parallel a$, the zero resistance can be observed up to 0.2 T at 1.8 K, while for $I \parallel b$, the superconductivity is dramatically suppressed in very small magnetic field. Note that an abnormal resistance peak is evident just above the critical temperature T_c^{onset} for $I \parallel b$, which can be found in the resistance curves of numerous nonhomogeneous superconducting films [22]. When the van der Pauw method is used to measure the resistance in a nonhomogeneous superconducting film, different regions of the film would exhibit slightly varied transition temperatures. While temperature is reduced, the nonuniform superconducting transition can lead to the uneven current distribution, resulting in a peaklike anomaly in the resistance curve. To measure the resistance for two orientations in the same sample, the electrode contact configuration shown in Fig. 1(d) was employed, which is similar to the van der Pauw method. The intrinsic anisotropic superconductivity in ZrTe$_3$ flakes might cause the nonuniform distribution of the current, which may lead to the anomaly peak in resistance. To validate this hypothesis, we also measured the resistance individually of another flake with the thickness of 18 nm for $I \parallel b$ by using the standard four-probe method, as shown in Fig. 4(c). No resistance anomaly is observed under different magnetic fields and the T_c^{zero} is consistent with that measured by the electrode contact

configuration in Fig. 1(d). To avoid any inaccuracies, T_c^{onset} will not be employed in subsequent analyses.

From Figs. 4(a) and 4(b), the pair-breaking mechanism can be analyzed by deducing the upper critical fields. Two different types of pair-breaking mechanisms can attribute to the suppression of superconductivity with the upper critical field, i.e., the Pauli paramagnetic and orbital effects. The former is originated from spin alignment by the sufficiently high external magnetic field [23]. When the field is high enough to match the Zeeman splitting energy with the bonding energy of a Cooper pair, the superconducting state can be broken. Thus the upper critical field can be defined as $\mu_0 H_p = \Delta/\sqrt{2}\mu_B = 1.84T_c$ for BCS superconductors, where μ_B is the Bohr magneton and $\Delta = 1.76k_BT_c$ is the BCS energy gap. We define the upper critical field $H_{c2}(R = 0.5R_n)$ and substitute $T_c = 4.45$ K with $I \parallel a$, and then $\mu_0 H_p$ is estimated as 8 T, significantly higher than the measured H_{c2}. So the orbital effect should be the dominant pair-breaking mechanism. This mechanism arises from the coupling between the magnetic field and the electron momentum. The H_{c2} can be fitted using the empirical formula derived from Ginzburg-Landau (GL) theory [24], expressed as

$$H_{c2}(T) = H_{c2}^{orb}(0)\frac{1 - t^2}{1 + t^2}, \qquad (1)$$

where t is the reduced temperature T/T_c, and $H_{c2}^{orb}(0)$ can be determined by the orbital effect at $T = 0$ K as

$$\mu_0 H_{c2}^{orb}(0) = -0.69T_c\left(\frac{\mu_0 dH_{c2}}{dT}\right). \qquad (2)$$

As shown in Fig. 4(d), the measured data can be well fitted by adopting the GL model [Eqs. (1) and (2)], indicating that the orbital effect primarily contributes to the suppression of both the bulk and filamentary superconductivity in an external magnetic field. For $I \parallel a$, $T_c(R = 0.5R_n) = 4.45$ K and the slope $\frac{\mu_0 dH_{c2}}{dT}$ at T_c is about -0.353 T/K, so that the estimated $H_{c2}^{orb}(0)$ is 1.09 T. For $I \parallel b$, $T_c(R = 0.5R_n) = 4$ K and the slope $\frac{\mu_0 dH_{c2}}{dT}$ at T_c is about -0.016 T/K, so that the estimated $H_{c2}^{orb}(0)$ is 0.045 T. Additionally, $H_{c2}(R = 0.1R_n)$ was fitted for comparison, as shown in Fig. 4(d).

In the context of a filamentary superconductor, a model based on GL theory proposes that the filaments can be either coupled or isolated [25]. If the superconducting filaments can interact via Josephson coupling, the I path can be enclosed and H_{c2} should be proportional to $|(T - T_c)/T_c|$ near T_c, which is close to the H_{c2} curves in Fig. 4(d). So superconductivity in ZrTe$_3$ along the b axis should be a result of the coupled superconducting filaments. With decreasing temperature, local pairs form along the a axis, related to the filamentary superconductivity. Then the phase coherence gradually develops upon further cooling and the superconducting filaments become coupled through the Josephson effect (where the resistance along the b axis begins to drop). However, the superconducting transition temperature of R_b is much lower than that of R_a and the coherence length suggested by the specific heat measurement is extremely short [9], which means that the Josephson coupling (along the b axis) can be easily broken by a magnetic field. Consequently, the superconductivity along the b axis is very sensitive to the external magnetic field.
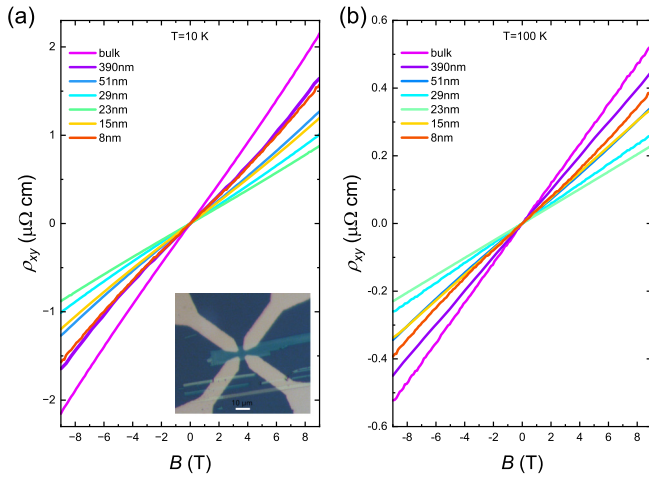
FIG. 5. (a), (b) Field dependence of Hall resistivity at representative thicknesses of $ZrTe_3$ above the CDW transition temperature (a) and below the CDW transition temperature (b). Inset is the schematic illustration of the $ZrTe_3$ thin flake device for Hall measurements; the irrelevant samples were then cut apart by the AFM needle tip.

To further investigate the intrinsic variation of electronic states with thickness, Hall resistivity ρ_{xy} of various $ZrTe_3$ flakes was measured with magnetic field applied along the c axis. Figures 5(a) and 5(b) exhibit the representative ρ_{xy} plotted against a magnetic field for several typical thicknesses at 10 and 100 K. ρ_{xy} is almost linearly dependent on magnetic field up to 9 T (the value of the subordinate carrier density estimated by the two-band model is two orders of magnitude smaller than that of dominant carrier density, rendering the minor nonlinearity in ρ_{xy} of 390 nm and 8 nm samples negligible) and the positive Hall coefficient indicates that the carriers are hole type for all samples, similar to the previous works [26]. The volumetric charge carrier density (n) is derived from the Hall data. The hole concentration n at 100 K (above T_{CDW}) is several times larger than that at 10 K (below T_{CDW}), yet they exhibit similar evolution against thickness.

In order to clarify the evolution of the superconducting as well as the CDW with the variation of flake thickness, a temperature-thickness phase diagram is constructed based on the above data. As shown in Fig. 6(a), the CDW and
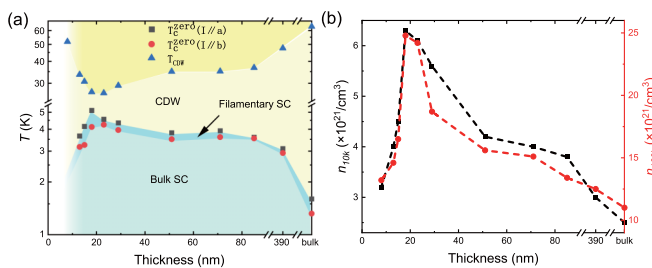
FIG. 6. (a) Temperature-thickness phase diagram of $ZrTe_3$. The triangles, squares, and circles indicate T_{CDW}, $T_c^{zero}(I \parallel a)$, and $T_c^{zero}(I \parallel b)$, respectively. (b) Thickness-dependent carrier densities at 100 K and 10 K. The volumetric charge carrier density (n) is determined by the Hall measurements at high field.

superconductivity exhibit opposite trends against thickness, indicating a competitive interaction in all the flakes, consistent with previous experiments taken with varying high pressure and doping [14–17]. When the thickness is thinned from bulk to around 18 nm, T_c^{zero} for both two directions increases, with the maximum T_c^{zero} reaching 5 K, more than three times higher than that in bulk crystal. Conversely, when the flakes is further thinned down from 18 nm, T_c^{zero} rapidly drops and T_{CDW} arises. The carrier densities n (10 K) and n (100 K) as functions of thickness are shown in Fig. 6(b). The hole concentration varies significantly with the reduction of thickness, first increasing and then dramatically decreasing, suggesting that thickness variation substantially influences the electronic structure. And the opposite trends of n and T_{CDW} against thickness indicate that the enhanced carrier density is conducive to superconductivity but detrimental to CDW formation.

Now we try to understand the competitive relation between CDW and superconductivity. Recent ARPES measurements showed that the Q1D FSs of $ZrTe_3$ are responsible for the CDW state and superconductivity [11,12]. The dominant character of the Q1D electronlike FSs is Te $5p_x$, which originates from the Te(2)-Te(3) chains along the a or c axis. First-principles calculations revealed that the detailed band structure of $ZrTe_3$ can be modulated by modifying the lattice constant c. Recent works showed that Cu and Ni intercalations in the van der Waals gap of $ZrTe_3$ could lead to a tensile lattice deformation of the Te(2)-Te(3) chains resulting in the expansion of the unit cell [13]. The reduction of phonon energy caused by the expansionary lattice constant c would reduce the electron-phonon coupling of the Q1D FS and consequently suppress the CDW. For few-layered van der Waals materials, a similar increase of interlayer lattice constant occurs due to the weakened interlayer coupling. The layer-dependent band gap of MoS_2 has been considered as a result of the evolution of structural parameters with thinning down [27,28]. The gradually weakened interlayer coupling strength might even decouple the in-plane and out-of-plane CDW ordering in a certain thickness, which would in turn enhance T_{CDW} with further decreasing thickness [29]. The opposite variation trends of carrier density and CDW transition temperature against thickness might imply that the shift of Fermi level upon thinning is responsible for the decrease of T_{CDW} and the enhancement of superconductivity in flakes thicker than 18 nm. However, given that the rapid rise of T_c^{zero} and reduction of T_{CDW} starts in the flake as thick as 390 nm (often considered as a bulk crystal), we cannot provide a definitive understanding of the pronounced changes in electronic states as the sample thickness varies from several micrometers to 390 nm. Comprehensive microscopic studies (including both crystal and electronic structure) should be required.

Next we turn to the transformation of electronic properties in flakes thinner than 18 nm. The suppression of superconductivity and the semiconducting behavior in $ZrTe_3$ flakes thinner than 18 nm might be ascribed to the enhanced strain resulting from the interaction between $ZrTe_3$ flakes and the substrates. Strain from the substrates can dramatically modulate physical properties in film systems. It has been reported that in few-layer $NbSe_2$ grown by molecular beam epitaxy, strain from the sapphire substrate has significant effects on its superconductivity and CDW [30]. The strain is induced by the mismatch of

the different lattice constants during the epitaxial growth. By varying the growth temperature, the compressive strain could be tuned. The superconductivity of NbSe$_2$ film was gradually suppressed and finally the film became an insulator. In our previous work, we found that when FeSe flakes on SiO$_2$ or Al$_2$O$_3$ substrates are thinner than a certain thickness between 13 and 27 nm, the evolution of superconductivity is distinct from that in thicker flakes, which possibly results from the strain effect from substrate on the ultrathin FeSe flakes [31]. For the exfoliated ZrTe$_3$ flakes here, the strain is absent at room temperature as the flakes were shifted on the substrates. However, due to the differing thermal expansion coefficients of the substrates and ZrTe$_3$ flakes, strain emerges upon cooling. The thermal shrinkage of SiO$_2$ and Al$_2$O$_3$ are isotropic along a and b axes as cooling down, resulting in identical relative length changes along these two directions for both SiO$_2$ and Al$_2$O$_3$ [32,33]. However, ZrTe$_3$ is monoclinic and its thermal expansion coefficient is anisotropic along monoclinic a and b axes [34]. In this case, ZrTe$_3$ flakes stuck on the SiO$_2$ or Al$_2$O$_3$ substrates will inevitably experience strain when temperature decreases. Employing density functional theory (DFT) computation, some reports predicted that the ZrTe$_3$ flake should be a metal down to monolayer, but would transform to a semiconductor with an indirect band gap when subjected to strain [35–37]. It should be pointed out that the observable effects of such strains on the electronic properties of ZrTe$_3$ flakes become evident only when the flakes are sufficiently thin, because the strain will be released in thicker flakes [38]. The rapid decrease of both T_c and carrier concentration as thickness <18 nm might be interpreted that the strain begins to take effect below this threshold. The amplified effect of disorder scattering as thickness approaching to the two-dimensional limit might be a plausible explanation for semiconducting behavior when thickness is reduced from 8 to 4 nm [39,40]. Another possible consideration could be the strongly correlated effect arising from the dominating electron-electron interaction over other electronic energy scales in the extreme two-dimensional limit, which has recently been thought to drive the metallic 1T-TaSe$_2$ into a Mott insulator by reducing the dimensionality [41].

IV. CONCLUSION

We have successfully obtained a series of ZrTe$_3$ flakes with different thickness by traditional mechanical and Al$_2$O$_3$-assisted exfoliation techniques and systematically investigated the evolution of transport properties of ZrTe$_3$ thin flakes down to bilayer with the current parallel to the a or b axis. While decreasing thickness, the CDW transition temperature with the current along the a axis first decreases from 63 K in bulk to a minimum of 27 K at thickness of 18 nm, then increases to 53 K as the thickness is further reduced to 8 nm. The superconducting transition temperature with current applied along both a and b axes varying against carrier density shows diametrically opposite trends compared to the CDW transition temperature, indicating a competitive relationship between CDW and superconductivity. Shifting of Fermi level upon thinning down, the anisotropic strain from the substrates and the increase of two-dimensional disorder scattering could account for the observed phenomena. Our work reveals a similar nonmonotonic evolution of the CDW and superconducting transition temperature with a reduction of thickness to the recently discovered layered kagome metal CsV$_3$Sb$_5$ [29], which might indicate a complicated superconducting mechanism. Further detailed microscopic studies are required for understanding the above results, especially the obvious increase of carrier density and superconducting transition temperature accompanied with the decrease of T_{CDW} caused by the thinning from bulk crystal to a flake thickness of 390 nm.

[1] G. Grüner, The dynamics of charge-density waves, Rev. Mod. Phys. **60**, 1129 (1988).

[2] A. H. C. Neto, Charge density wave, superconductivity, and anomalous metallic behavior in 2D transition metal dichalcogenides, Phys. Rev. Lett. **86**, 4382 (2001).

[3] H. Barath, M. Kim, J. F. Karpus, S. L. Cooper, P. Abbamonte, E. Fradkin, E. Morosan, and R. J. Cava, Quantum and classical mode softening near the charge-density-wave–superconductor transition of Cu$_x$TiSe$_2$, Phys. Rev. Lett. **100**, 106402 (2008).

[4] Y. I. Joe, X. M. Chen, P. Ghaemi, K. D. Finkelstein, G. A. de la Pena, Y. Gan, J. C. T. Lee, S. Yuan, J. Geck, G. J. MacDougall, T. C. Chiang, S. L. Cooper, E. Fradkin, and P. Abbamonte, Emergence of charge density wave domain walls above the superconducting dome in 1T-TiSe$_2$, Nat. Phys. **10**, 421 (2014).

[5] K. Stöwe and F. R. Wagner, Crystal structure and calculated electronic band structure of ZrTe$_3$, J. Solid State Chem. **138**, 160 (1998).

[6] P. Starowicz, C. Battaglia, F. Clerc, L. Despont, A. Prodan, H. van Midden, U. Szerer, A. Szytuła, M. G. Garnier, and P. Aebi, Electronic structure of ZrTe$_3$, J. Alloys Compd. **442**, 268 (2007).

[7] S. P. Lyu, L. Yu, J. W. Huang, C. T. Lin, Q. Gao, J. Liu, G. D. Liu, L. Zhao, J. Yuan, and C. T. Chen, Detailed electronic structure of three-dimensional Fermi surface and its sensitivity to charge density wave transition in ZrTe$_3$ revealed by high resolution laser-based angle-resolved photoemission spectroscopy, Chin. Phys. B **27**, 087503 (2018).

[8] H. Nakajima, K. Nomura, and T. Sambongi, Anisotropic superconducting transition in ZrTe$_3$, Physica B+C (Amsterdam) **143**, 240 (1986).

[9] K. Yamaya, S. Takayanagi, and S. Tanda, Mixed bulk-filament nature in superconductivity of the charge-density-wave conductor ZrTe$_3$, Phys. Rev. B **85**, 184513 (2012).

[10] S. Tsuchiya, K. Matsubayashi, K. Yamaya, S. Takayanagi, S. Tanda, and Y. Uwatoko, Effects of pressure and magnetic field

on superconductivity in ZrTe$_3$: Local pair-induced superconductivity, New J. Phys. **19**, 063004 (2017).

[11] T. Yokoya, T. Kiss, A. Chainani, S. Shin, and K. Yamaya, Role of charge-density-wave fluctuations on the spectral function in a metallic charge-density-wave system, Phys. Rev. B **71**, 140504(R) (2005).

[12] M. Hoesch, X. Y. Cui, K. Shimada, C. Battaglia, S. Fujimori, and H. Berger, Splitting in the Fermi surface of ZrTe$_3$: A surface charge density wave system, Phys. Rev. B **80**, 075423 (2009).

[13] Y. Liu, X. Tong, V. N. Ivanovski, Z. X. Hu, D. Leshchev, X. D. Zhu, H. C. Lei, E. Stavitski, K. Attenkofer, and V. Koteski, Enhanced superconductivity and electron correlations in intercalated ZrTe$_3$, Phys. Rev. B **106**, 165113 (2022).

[14] K. Yamaya, M. Yoneda, S. Yasuzuka, Y. Okajima, and S. Tanda, The effect of pressure on the charge-density wave and superconductivity in ZrTe$_3$, J. Phys.: Condens. Matter **14**, 10767 (2002).

[15] X. D. Zhu, W. Ning, L. J. Li, L. S. Ling, R. R. Zhang, J. L. Zhang, K. F. Wang, Y. Liu, L. Pi, and Y. C. Ma, Superconductivity and charge density wave in ZrTe$_{3-x}$Se$_x$, Sci. Rep. **6**, 26974 (2016).

[16] H. C. Lei, X. D. Zhu, and C. Petrovic, Raising T_c in charge density wave superconductor ZrTe$_3$ by Ni intercalation, Europhys. Lett. **95**, 17011 (2011).

[17] R. Yomo, K. Yamaya, M. Abliz, M. Hedo, and Y. Uwatoko, Pressure effect on competition between charge density wave and superconductivity in ZrTe$_3$: Appearance of pressure-induced reentrant superconductivity, Phys. Rev. B **71**, 132508 (2005).

[18] X. D. Zhu, H. C. Lei, and C. Petrovic, Coexistence of bulk superconductivity and charge density wave in Cu$_x$ZrTe$_3$, Phys. Rev. Lett. **106**, 246404 (2011).

[19] Y. J. Deng, Y. J. Yu, Y. C. Song, J. Z. Zhang, N. Z. Wang, Z. Y. Sun, Y. F. Yi, Y. Z. Wu, S. W. Wu, and J. Y. Zhu, Gate-tunable room-temperature ferromagnetism in two-dimensional Fe$_3$GeTe$_2$, Nature (London) **563**, 94 (2018).

[20] S. Manzeli, D. Ovchinnikov, D. Pasquier, O. V. Yazyev, and A. Kis, 2D transition metal dichalcogenides, Nat. Rev. Mater. **2**, 17033 (2017).

[21] X. Y. Zhu, B. Lv, F. Y. Wei, Y. Y. Xue, B. Lorenz, L. Z. Deng, Y. Y. Sun, and C. W. Chu, Disorder-induced bulk superconductivity in ZrTe$_3$ single crystals via growth control, Phys. Rev. B **87**, 024508 (2013).

[22] R. Vaglio, C. Attanasio, L. Maritato, and A. Ruosi, Explanation of the resistance-peak anomaly in nonhomogeneous superconductors, Phys. Rev. B **47**, 15302 (1993).

[23] A. M. Clogston, Upper limit for the critical field in hard superconductors, Phys. Rev. Lett. **9**, 266 (1962).

[24] N. R. Werthamer, E. F. Helfand, and P. C. Hohenberg, Temperature and purity dependence of the superconducting critical field, H_{c2}. III. Electron spin and spin-orbit effects, Phys. Rev. **147**, 295 (1966).

[25] L. A. Turkevich and R. A. Klemm, Ginzburg-Landau theory of the upper critical field in filamentary superconductors, Phys. Rev. B **19**, 2520 (1979).

[26] S. Takahashi, T. Sambongi, J. W. Brill, and W. Roark, Transport and elastic anomalies in ZrTe$_3$, Solid State Commun. **49**, 1031 (1984).

[27] Y. C. Cheng, Z. Y. Zhu, and U. Schwingenschlögl, Role of interlayer coupling in ultra thin MoS$_2$, RSC Adv. **2**, 7798 (2012).

[28] C. Lee, H. Yan, L. E. Brus, T. F. Heinz, J. Hone, and S. Ryu, Anomalous lattice vibrations of single-and few-layer MoS$_2$, ACS Nano **4**, 2695 (2010).

[29] B. Q. Song, T. P. Ying, X. X. Wu, W. Xia, Q. W. Yin, Q. H. Zhang, Y. P. Song, X. F. Yang, J. G. Guo, L. Gu, X. L. Chen, J. P. Hu, A. P. Schnyder, H. C. Lei, Y. F. Guo, and S. Y. Li, Anomalous enhancement of charge density wave in kagome superconductor CsV$_3$Sb$_5$ approaching the 2D limit, Nat. Commun. **14**, 2492 (2023).

[30] C. Chen, P. Das, E. Aytan, W. M. Zhou, J. Horowitz, B. Satpati, A. A. Balandin, R. K. Lake, and P. Wei, Strain-controlled superconductivity in few-layer NbSe$_2$, ACS Appl. Mater. Interfaces **12**, 38744 (2020).

[31] C. S. Zhu, B. Lei, Z. L. Sun, J. H. Cui, M. Z. Shi, W. Z. Zhuo, X. G. Luo, and X. H. Chen, Evolution of transport properties in FeSe thin flakes with thickness approaching the two-dimensional limit, Phys. Rev. B **104**, 024509 (2021).

[32] M. Lucht, M. Lerche, H.-C. Wille, Y. V. Shvyd'ko, H. D. Rüter, E. Gerdau, and P. Becker, Precise measurement of the lattice parameters of α-Al$_2$O$_3$ in the temperature range 4.5–250 K using the Mössbauer wavelength standard, J. Appl. Crystallogr. **36**, 1075 (2003).

[33] G. A. Lager, J. D. Jorgensen, and F. J. Rotella, Crystal structure and thermal expansion of α-quartz SiO$_2$ at low temperatures, J. Appl. Phys. **53**, 6751 (1982).

[34] S. Furuseth and H. Fjellvag, Reexamination of the crystal-structure of ZrTe$_3$, Acta Chem. Scand. **45**, 694 (1991).

[35] Y. D. Jin, X. X. Li, and J. L. Yang, Single layer of MX$_3$ (M= Ti, Zr; X= S, Se, Te): a new platform for nano-electronics and optics, Phys. Chem. Chem. Phys. **17**, 18665 (2015).

[36] B. Mortazavi, F. Shojaei, M. Yagmurcukardes, M. Makaremi, and X. Y. Zhuang, A theoretical investigation on the physical properties of zirconium trichalcogenides, ZrS$_3$, ZrSe$_3$ and ZrTe$_3$ monolayers, Energies **15**, 5479 (2022).

[37] M. Li, J. Dai, and X. C. Zeng, Tuning the electronic properties of transition-metal trichalcogenides via tensile strain, Nanoscale **7**, 15385 (2015).

[38] S. Y. Tan, Y. Zhang, M. Xia, Z. R. Ye, F. Chen, X. Xie, R. Peng, D. F. Xu, Q. Fan, H. C. Xu, J. Jiang, T. Zhang, X. C. Lai, T. Xiang, J. P. Hu, B. P. Xie, and D. L. Feng, Interface-induced superconductivity and strain-dependent spin density waves in FeSe/SrTiO$_3$ thin films, Nat. Mater. **12**, 634 (2013).

[39] A. D. Zaikin, D. S. Golubev, A. van Otterlo, and G. T. Zimányi, Quantum phase slips and transport in ultrathin superconducting wires, Phys. Rev. Lett. **78**, 1552 (1997).

[40] Z. L. Liao, F. M. Li, P. Gao, L. Li, J. D. Guo, X. Q. Pan, R. Jin, E. W. Plummer, and J. D. Zhang, Origin of the metal-insulator transition in ultrathin films of La$_{2/3}$Sr$_{1/3}$MnO$_3$, Phys. Rev. B **92**, 125123 (2015).

[41] N. Tian, Z. Huang, B. G. Jang, S. Guo, Y. J. Yan, J. J. Gao, Y. J. Yu, J. Hwang, C. Y. Tang, M. X. Wang, X. Luo, Yu. P. Sun, Z. K. Liu, D. L. Feng, X. H. Chen, S. K. Mo, Y. M. Kim, Y. W. Son, D. W. Shen, W. Ruan, and Y. B. Zhang, Dimensionality-driven metal to Mott insulator transition in two-dimensional 1T-TaSe$_2$, Natl. Sci. Rev. **11**, nwad144 (2024).